# THE EVOLUTION OF ACTIVE GALACTIC NUCLEI IN WARM DARK MATTER COSMOLOGY

N. MENCI, F. FIORE, AND A. LAMASTRA
INAF, Osservatorio Astronomico di Roma, via di Frascati 33, I-00040 Monteporzio, Italy

## ABSTRACT

Recent measurements of the abundance of active galactic nuclei (AGNs) with low luminosities ($L_{2-10} \leqslant 10^{44}$ erg s$^{-1}$ in the 2–10 keV energy band) at high redshifts ($z \geqslant 4$) provide a serious challenge for cold dark matter (CDM) models based on interaction-driven fueling of AGNs. Using a semi-analytic model of galaxy formation we investigate how such observations fit in a warm dark matter (WDM) scenario of galaxy formation, and compare the results with those obtained in the standard CDM scenario with different efficiencies for the stellar feedback. Taking on our previous exploration of galaxy formation in WDM cosmology, we assume as a reference case a spectrum which is suppressed—compared to the standard CDM case—below a cutoff scale ≈0.2 Mpc corresponding (for thermal relic WDM particles) to a mass $m_X = 0.75$ keV. We run our fiducial semi-analytic model with such a WDM spectrum to derive AGN luminosity functions from $z \approx 6$ to the present over a wide range of luminosities ($10^{43} \leqslant L_{2-10}/\mathrm{erg\ s}^{-1} \leqslant 10^{46}$ in the 2–10 keV X-ray band), to compare with recent observations and with the results in the CDM case. When compared with the standard CDM case, the luminosity distributions we obtain assuming a WDM spectrum are characterized by a similar behavior at low redshift, and by a flatter slope at faint magnitudes for $z \geqslant 3$, which provide an excellent fit to present observations. We discuss how such a result compares with CDM models with maximized feedback efficiency, and how future deep AGN surveys will allow for a better discrimination between feedback and cosmological effects on the evolution of AGNs in interaction-driven models for AGN fueling.

*Key words:* cosmology: theory – dark matter – galaxies: active – galaxies: formation

*Online-only material:* color figures

## 1. INTRODUCTION

Perhaps the most striking aspects of active galactic nuclei (AGNs) are their strong evolution with redshift, and the strong correlations between the properties of the AGN and those of their host galaxies. The former appears as a strong increase in their number and luminosities from $z = 0$ to $z = 3$ (see Hartwick & Shade 1990; Boyle et al. 2000; Ueda et al. 2003) followed by a decline in the number of AGNs at higher redshifts (Fan et al. 2001, 2004), while the latter involve, e.g., the correlations between the stellar mass (or the velocity dispersion of the bulge) of the host galaxy and the mass of the accreting black hole (BH) powering the AGN emission (Kormendy & Richstone 1995; Magorrian et al. 1998; Ho 1999; Gebhardt et al. 2000; Ferrarese & Merritt 2000; Marconi & Hunt 2003; Häring & Rix 2004; Kormendy & Bender 2009). Both such key features call for a cosmological explanation of the BH and AGN properties, which in fact constitutes one of the most pressing issues in astrophysics.

On the theoretical side, models aimed at describing the evolution of BHs and AGNs in a cosmological context are based on either *N*-body simulations and semi-analytic models. While the former have shown the importance of galaxy mergers as triggers for AGN accretion and the role of the AGN energy feedback in the subsequent evolution of the host galaxy (see, e.g., Di Matteo et al. 2005; Springel 2005; Hopkins et al. 2005a, 2006), the evolution of the statistical properties of AGNs in a cosmological context has been mainly investigated through SAM (see Baugh 2006 for a review), which allow a faster spanning of the parameter space compared to *N*-body simulations. In fact, they adopt analytic laws to connect the evolution of dark matter (DM) halos collapsed from the primordial density field and their subsequent merging histories (derived from Monte Carlo or *N*-body simulations) to the physics of

baryons inside the halos, including the gas processes, the star formation, and the growth of supermassive BHs due to gas accretion and merging (see Kauffmann & Haehnelt 2000; Menci et al. 2003, 2006; Croton et al. 2006; Bower et al. 2006; Cattaneo et al. 2006; Hopkins et al. 2006; Monaco et al. 2007; Marulli et al. 2008).

Besides some variance concerning the role of minor interactions and the implementation of the AGN feedback, quenching the star formation in the host galaxy, all such models include galaxy interactions as triggers for gas accretion onto the BHs; observationally, this is motivated by the ULRIG–QSO connection (Sanders & Mirabel 1996; Canalizo & Stockton 2001), the signature of recent mergers in QSO hosts (see, e.g., Bennert et al. 2008; Treister et al. 2012), and the small-scale overdensities around luminous QSOs (see Fisher et al. 1996; Bahcall et al. 1997; Serber et al. 2006; Hennawi et al. 2006; Myers et al. 2008; Strand et al. 2008). Based on the assumption of interaction-triggered QSOs, complemented with the inclusion of accretion of hot gas (Bower et al. 2006; Croton et al. 2006) and of disk instabilities as additional triggers (see Fanidakis et al. 2012; Hirschmann et al. 2012), several state-of-the-art cosmological models correctly describe the tight correlation between galaxy properties and BH mass (Hopkins et al. 2008; Marulli et al. 2008; Somerville et al. 2008; Lamastra et al. 2010; Guo et al. 2011) and the evolution of luminous QSO population over a wide range of cosmic ages (see Menci et al. 2003, 2006; Hopkins et al. 2008; Shankar et al. 2010; Fanidakis et al. 2012; Hirschmann et al. 2012). These successes allowed the models to provide a cosmological interpretation of the observed luminosity-dependent evolution of AGNs (the "downsizing" effect): on the one hand, the strong evolution of the bright QSO population observed in optical surveys (see Richards et al. 2006; Croom et al. 2009; Glikman et al. 2011; Jiang et al. 2009)

results from the combination of the time-decline of merging activity and of the exhaustion of the cold gas content in massive galaxy halos due to the its early conversion into stars at high redshifts; on the other hand, the smoother evolution with redshift of the observed abundance of low-luminosity AGNs revealed mainly by X-ray surveys (effectively probing such a population; see, e.g., Hasinger et al. 2005; La Franca et al. 2005; Fiore et al. 2012 and discussion therein) results from the milder evolution of the gas content in low-mass galaxies predicted by the models and the early collapse epoch of the corresponding host DM clumps envisaged in the standard cold dark matter (CDM) cosmology.

However, while for bright QSOs and for low-redshift AGNs the predicted evolution and downsizing agree with measurements from optical and X-ray surveys (see Menci et al. 2008; Hopkins et al. 2008; Shen 2009; Shankar et al. 2010), the recent observational breakthroughs concerning the abundance of faint AGNs at high redshifts ($z \gtrsim$ 3–5) are posing serious challenges to the cosmological models for the AGN evolution. Indeed, recent estimates of the X-ray luminosity functions of AGNs extending down to $\log L$ (2–10 keV) $\approx 42.75$ (Fiore et al. 2012) are in sharp contrast with the large density of faint AGNs predicted by analytic (Shankar et al. 2010) or semi-analytic (Menci et al. 2006, 2008) models for the coevolution of galaxies and AGNs (see also Shankar & Mathur 2007; Wyithe & Loeb 2003; Lapi et al. 2006), even when the observed luminosity functions are corrected for the estimated fraction of obscured objects (e.g., La Franca et al. 2005), the models predicting up to ten times more AGNs with X-ray luminosity $L_X \leqslant 10^{43}$ erg s$^{-1}$ (in the 2–10 keV band). Results from other last-generation semi-analytic models based on merging trees extracted from $N$-body simulations (Marulli et al. 2008) or on Monte Carlo generated merging trees (Hirschmann et al. 2012) confirm the mismatch. In fact, although the above papers also assume disk instabilities provide additional triggers, they yield high-redshift ($z \gtrsim 4$) AGN luminosity functions steeper than the observed ones, so that they cannot provide a simultaneous fit to both the number density of bright QSOs (measured by the SLOAN survey) and the abundance of lower luminosity AGNs (detected from hard X-ray measurements), unless tuned, non-canonical assumptions (such as heavy BH seeds, a varying sub-Eddington limit, and a halo mass limit) are adopted (Hirschmann et al. 2012). The indication is that, when tuned to account for the observed high abundance of low-redshift faint AGNs and of bright QSOs at high redshifts, *most* semi-analytic models based on CDM are characterized by an overprediction of faint AGNs at $z \gtrsim 4$. Note however that the possibility that the CDM models of AGN evolution may be brought in agreement with the observations by a proper implementation of the baryon physics is still open; in fact, the AGN luminosity functions derived in the CDM semi-analytic model by Fanidakis et al. (2012) have a flatter slope at the faint end as to be consistent with the observations (including those concerning the X-ray luminosity distributions after their modeling of the fraction of obscured objects).

Such an overprediction of faint objects, especially at high redshifts, is indeed a common and robust feature of CDM galaxy formation models. In fact, the latter yield galaxy luminosity functions largely exceeding those measured in $K$-band for $0 \lesssim z \lesssim 3$ (see Cirasuolo et al. 2010; Henriques et al. 2011) or those corresponding to faint Lyman-break galaxies (Lo Faro et al. 2009) at $z \gtrsim 3$; the excess of star-forming low-mass galaxies at $z \gtrsim 3$ reflects an excess of red low-mass galaxies at $z \approx 0$ (see, e.g., Croton et al. 2006; Salimbeni et al.

2008). Analogously, the number of galaxies with stellar mass $M_* \lesssim 10^{10} M_\odot$ in the universe is systematically overpredicted by all theoretical CDM models (Fontana et al. 2006; Fontanot et al. 2009; Marchesini et al. 2009; Guo et al. 2011) in the whole range $1 \lesssim z \lesssim 3$ where the small-mass end of the mass function has been measured (see also Santini et al. 2012).

While it is possible that AGN feeding mechanisms not based on galaxy interaction (see Ciotti 2009; Shin et al. 2010; see also Treister et al. 2012 for the relative role of merging and secular processes) may be at the origin of the mismatch, the dominating point of view is that all models miss some kind of process involved in the complex baryonic physics describing galaxy formation and AGN evolution (see, e.g., Somerville et al. 2008). In particular, models could fail to properly describe the feedback processes such as heating or winds caused by supernova explosions and UV background, which may be effective in expelling gas in shallow potential wells, thus suppressing both star formation and BH growth in low-mass galaxies. In present models the effectiveness of such a solution is limited by the large densities of DM halos formed at high redshift, which allow for an effective shielding of the inner regions and yield escape velocities larger than the kinetic energy of SN-driven winds (see discussion in Lo Faro et al. 2009).

An alternative possibility is that the conflicts are rooted in the CDM spectrum assumed by all the above cosmological models of galaxy formation and AGN evolution. Indeed, the shape of the CDM spectrum of density perturbations, ultimately determining the abundance and the merging histories of DM halos, is constrained by present observations only for mass scales exceeding $M \approx 10^9 M_\odot$, corresponding to scales $r \gtrsim 0.3$ Mpc effectively probed by the comparison of the Ly$\alpha$ forest spectra at $z \approx 2.5$ with the $N$-body simulations (Viel et al. 2005, 2008). On smaller mass scales, a strong suppression in the DM spectrum would still be consistent with present observations; physically, such a suppression could be achieved by assuming DM to be constituted by particles with mass $m_X \approx 1$ keV, characterized by large thermal speeds $v_s/c \approx 0.2$ (warm dark matter, WDM; see Peebles 1982; Bond et al. 1982; Colombi et al. 1996 and references therein; see also de Vega & Sanchez 2012) corresponding to a free-streaming scale $r_{fs} \sim v_s t_{eq} \approx 0.2$ Mpc (here $t_{eq}$ is the time of matter-radiation equality). An effective suppression of the DM power spectrum at small scales could indeed provide a viable solution to several long-standing tensions between the CDM predictions and the observations, like the low number of satellites within the halos of galaxies and groups compared to CDM model predictions (see Klypin et al. 1999; Moore et al. 1999; see also Mateo 1998; Lovell et al. 2012) and the observed inner density profiles of galaxies inferred from rotation curves of real galaxies which are flatter than those resulting in CDM $N$-body simulations (Moore et al. 1999; Abadi et al. 2003; Reed et al. 2005; Madau et al. 2008; for observations see, e.g., Gentile et al. 2007; McGaugh et al. 2007).

In a previous paper (Menci et al. 2012, Paper I) we investigated for the first time the effects of a WDM power spectrum on the statistical properties of galaxies using our semi-analytic model of galaxy formation, and we showed that assuming WDM cold alleviate the discrepancy between the observed and the predicted galaxy luminosity and stellar mass distributions. Here we take on our previous study to explore the evolution of AGNs in a WDM context; we focus on the evolution of the AGN luminosity function from the highest redshift where observations are available ($z \approx 6$) to the present, and we compare with

state-of-the-art observational data and with our previous predictions based on the standard CDM cosmology.

## 2. METHOD

We use the method adopted in Paper I to investigate the effects of the WDM power spectrum on galaxy formation. We adopt the Rome semi-analytic model (R-SAM) to connect the physical processes involving baryons (physics of gas, star formation, feedback, growth of supermassive BHs) to the merging histories of DM halos, ultimately determined by the DM initial power spectrum. The model free parameters, including the cosmological ones, are set as in Menci et al. (2005, 2006, 2008); the only change is that merging trees are now computed in a WDM cosmology. This allows us to single out the effects of changing the DM spectrum with the same baryon physics and cosmological framework. Here we briefly recall the basic features of the model (for a complete description see Menci et al. 2005, 2006, 2008), and we describe the power spectrum we use to compute the merging trees in the WDM cosmology.

### 2.1. The Semi-analytic Model: The History of Dark Matter Halos in CDM and WDM Cosmology

Galaxy formation and evolution is driven by the collapse and growth of DM halos, which originate from the gravitational instability of overdense regions in the primordial density field. This is taken to be a random, Gaussian density field within the "concordance cosmology" (Spergel et al. 2007), for which we adopt round parameters $\Omega_\Lambda = 0.7$, total matter density parameter $\Omega_M = 0.3$ (with baryon contribution corresponding to $\Omega_b = 0.04$), and Hubble constant (in units of $100$ km s$^{-1}$ Mpc$^{-1}$) $h = 0.7$. The normalization of the spectrum is taken to be $\sigma_8 = 0.9$ in terms of the variance of the field smoothed over regions of $8\ h^{-1}$ Mpc. Adopting the exact best fit WMAP7 values for the above parameters does not change our results appreciably.

As cosmic time increases, larger and larger regions of the density field collapse, and eventually lead to the formation of groups and clusters of galaxies; previously formed, galactic-size condensations are enclosed. The statistical properties and the merging history of DM halos depend on the variance of the primordial DM density field as a function of the smoothing mass scale:

$$\sigma^2(M) = \int \frac{dk\, k^2}{2\,\pi^2}\, P(k)\, W(kr), \qquad (1)$$

where $P(k)$ is the linear power spectrum of DM perturbations at a wavelengths $k = 2\pi/r$, $M \simeq 1.2\,10^{12}\, h^2\, M_\odot\, (r/\mathrm{Mpc})^3$ is the mass within a sphere of radius $r$, and $W$ is a window function (see Peebles 1993), usually assumed to be top-hat in real space. Thus, the linear power spectrum $P(k)$ determines the merging histories and the mass distribution of DM halos. For the CDM cosmology we adopt the form $P_{\mathrm{CDM}}(k)$ given by Bardeen et al. (1986). The WDM spectrum is suppressed with respect to the CDM case below a characteristic scale depending on the mass of the WDM particles (and, for non-thermal particles, also on their mode of production; see Kusenko 2009); in fact, the large thermal velocities of the lighter WDM particles erase the perturbations with size comparable to and below the free-streaming scale $r_{fs}$. In the case where WDM is composed of relic thermalized particles, such a suppression is quantified through the ratio of the two linear power spectra (transfer function)

which can be parameterized as (Bode et al. 2001; see also Viel et al. 2005)

$$\frac{P_{\mathrm{WDM}}(k)}{P_{\mathrm{CDM}}(k)} = [1 + (\alpha\,k)^{2\,\mu}]^{-5\,\mu}\ \text{with}\ \alpha = 0.049 \left[\frac{\Omega_X}{0.25}\right]^{0.11}$$

$$\times \left[\frac{m_X}{\mathrm{keV}}\right]^{-1.11} \left[\frac{h}{0.7}\right]^{1.22} h^{-1}\ \mathrm{Mpc}\ \text{and}\ \mu = 1.12 \qquad (2)$$

The above relation between transfer function and DM particle mass $m_X$ is valid for thermal relics; a similar relation holds for sterile neutrinos (if they are produced from oscillations with active neutrinos) provided one substitutes the mass $m_X$ with a mass $m_{\mathrm{sterile}} = 4.43\ \mathrm{KeV}\ (m_X/\mathrm{keV})^{4/3}\ (\Omega_{\mathrm{WDM}}\, h^2/0.1225)^{-1/3}$. In both cases, the smaller the WDM mass $m_X$ (or $m_{\mathrm{sterile}}$) the larger the suppression with respect to the standard CDM spectrum. We shall adopt as a reference case a WDM (thermal) particle mass $m_X = 0.75$ keV; this allows us to investigate the effects of the largest suppression of the DM power spectrum which is still consistent with the most stringent observational constraints $m_X \gtrsim 0.6$ keV (for thermal particles); these have been derived by Viel et al. (2005) by comparing the observed Ly$\alpha$ forest in absorption spectra of quasars at $z = 2$–$3$ with the results of $N$-body simulation runs assuming different WDM power spectra of perturbations. Adopting the above value for the WDM particle mass yields a suppression of the power spectrum (with respect to CDM) at scales below $r_{fs} \approx 0.2$ Mpc (see Paper I); correspondingly, the abundance and the probability of inclusion of DM halos with mass $M_{fs} \approx 5\,10^8\, M_\odot$ are suppressed (with respect to the CDM case), according to Equation (1).

The mass function and the progenitor distribution of DM halos (determining the merging history of the halos) can be derived from Equations (1) and (2) (see Barkana et al. 2001; Smith & Markovic 2011), assuming a threshold for collapse of DM halos given by the critical linear-theory overdensity of the collapse of top-hat perturbations. For the CDM case, a detailed framework for the computation of such quantities (the Extended Press & Schechter formalism, EPS hereafter) has been introduced by Bond et al. (1991; see also Lacey & Cole 1993), and later developed to improve the agreement with $N$-body simulations (see Sheth et al. 2001). For the WDM case, recent works (Benson et al. 2013) have shown that the choice of an appropriate window function $W$ (Equation (1)) and of the collapse threshold is non-trivial; the latter authors provide a generalized algorithm for computing the halo merger rates and the mass function in WDM cosmology where the threshold and the filter function are calibrated through $N$-body simulation. They found that, compared with a straightforward application of EPS with a WDM spectrum (Equation (2)), both the progenitor distribution and the mass function are strongly suppressed below the free-streaming scale $M_{fs}$. In Paper I we assumed the straightforward extension of the EPS to the WDM spectrum as a reference framework to compute the above quantities, and we bracketed the uncertainties concerning the window function and the collapse threshold by assuming a sharp cutoff for the progenitor distribution and the mass function at $M = M_{fs}$, a phenomenological (extreme) rendition of the findings of Benson et al. (2013). Here we retain such approach, and we shall show the WDM results on the AGN luminosity functions as bracketed between those corresponding to a straightforward application of the EPS and those corresponding to a merging history where the progenitor distributions (and correspondingly the halo mass

functions) are completely suppressed for masses $M \lesssim M_{fs}$; the detailed procedure adopted to generate Monte Carlo realizations of merger trees in both cases is described Section 4 of Paper I.

Following the canonical procedure adopted by SAMs, after generating Monte Carlo realizations of the DM merger trees, we follow the history of DM clumps included in larger DM halos; these may survive as satellites, or merge to form larger galaxies due to binary aggregations, or coalesce into the central dominant galaxy due to dynamical friction (see Menci et al. 2005, 2006). In addition satellite halos are partially disrupted as the density in their outer parts becomes lower than the density of the host halo within the pericenter of its orbit (see Menci et al. 2002 for details). Since the above galaxy coalescence processes take place over timescales that grow longer over cosmic time, the number of satellite galaxies increases as the DM host halos grow from groups to clusters.

### 2.2. The Semi-analytic Model: The Baryonic Physics and Evolution of AGNs

The SAMs relate the physics of baryons to the DM merging trees, determined by the DM power spectrum as discussed above.

The radiative gas cooling, the ensuing star formation, and the supernova events with the associated feedback occurring in the growing DM halos are computed for each sub-halo hosting a galaxy. The cooled gas with mass $m_c$ settles into a rotationally supported disk with radius $r_d$, rotation velocity $v_d$, and dynamical time $t_d = r_d/v_d$, all related to the DM sub-halo mass. The gas gradually condenses into stars at a rate $\dot{m}_* \propto m_c/t_d$. The ensuing stellar feedback returns part of the cooled gas to the hot gas phase at the virial temperature of the halo; from a simple energy balance argument, the mass rate of the gas returning to the hot phase can be estimated as $\dot{m}_{hot} = \epsilon_0 \eta_{SN} E_{SN}/v_{esc}^2$ (Dekel & Silk 1986; cf. Kauffmann et al. 1993; Natarajan 1999), where $v_{esc}$ is the galaxy escape velocity, $E_{SN} = 10^{51}$ erg is the energy released by a single supernova, $\eta_{SN}$ is the number of supernovae per unit stellar mass (for a Salpeter initial mass function $\eta_{SN} = 6.5 \, 10^{-3}$), and $\epsilon_0 \in [0, 1]$ is a tunable efficiency for the coupling of the emitted energy with the interstellar gas: in our fiducial model we set $\epsilon = 0.01$. An additional channel for star formation implemented in the model is provided by interaction-driven starbursts, triggered not only by merging but also by fly-by events between galaxies; such a star formation mode provides an important contribution to the early formation of stars in massive galaxies, as described in detail in Menci et al. (2003, 2005).

The R-SAM provides a detailed description of the growth of BHs inside each DM halo from primordial seeds with mass $M_{BH} \approx 10^2 \, M_\odot$ through merging between galaxies and accretion of a fraction of the cold galactic gas $m_c$. The accretion is triggered by galaxy interactions (i.e., minor and major merging, and fly-by events), and the fraction of cold gas funneled to the central BH is derived from the model by Cavaliere & Vittorini (2000). The active accretion phase of BHs corresponds to the AGN.

The accretion of cold gas is triggered by galaxy interactions, namely, fly-by encounters, and both minor and major merging events. In fact, all such kinds of interactions destabilize part of the available cold gas by inducing loss of angular momentum. In fact, small scale (0.1–a few kpc) regions are likely to have disk geometry if they are to efficiently remove angular momentum and convey to the (unresolved) parsec scales the gas provided on larger scales (these may be isotropized by head-on, major merging events). The fraction of cold gas accreted by the BH in an interaction event is computed in terms of the variation $\Delta j$ of the specific angular momentum $j \approx Gm/v_d$ of the gas, to read (Menci et al. 2003)

$$f_{acc} = 10^{-1} \left\langle \frac{m'}{m} \frac{r_d}{b} \frac{v_d}{V} \right\rangle. \tag{3}$$

Here $b$ is the impact parameter (evaluated as the average distance of the galaxies in the halo), $m'$ is the mass of the partner galaxy in the interaction, and the average runs over the probability of finding such a galaxy in the same host halo (with circular velocity $V$) where the galaxy with mass $m$ is located. The values of the quantities involved in the average yield $f_{acc} \lesssim 10^{-2}$. For minor merging events and for fly-by encounters among galaxies with very unequal mass ratios $m' \ll m$, dominating the statistics in all hierarchical models of galaxy formation, the accreted fraction takes values $10^{-3} \lesssim f_{acc} \lesssim 10^{-2}$. The average amount of cold gas accreted during an accretion episode is thus $\Delta m_{acc} = f_{acc} m_c$, and the duration of an accretion episode, i.e., the timescale for the QSO or AGN to shine, is assumed to be the crossing time $\tau = r_d/v_d$ for the destabilized cold gas component.

The rate of such interactions is given by Menci et al. (2003) in the form $\tau_r^{-1} = n_T \, \Sigma(m, m') \, V_{rel}$. Here $n_T$ is the number density of galaxies in the same host halo and $V_{rel} = \sqrt{2} \, V$ is their average relative velocity in the host halo with circular velocity $V$. The cross section $\Sigma$ for grazing encounters (effective for angular momentum transfer) is given by Saslaw (1985) in terms of the tidal radii associated with the two interacting partners with mass $m$ and $m'$ (see Menci et al. 2003, 2004). For each galaxy (with mass $m$) in the Monte Carlo realizations, and at each time step $\Delta t$, the probability to interact with a partner (with mass $m'$) in the same halo is estimated as $\Delta t/\tau_r(m, m')$.

For each galaxy during an interaction phase, the time-averaged bolometric luminosity so produced by a QSO hosted in a given galaxy is then computed as

$$L = \frac{\eta \, c^2 \Delta m_{acc}}{\tau}. \tag{4}$$

We adopt an energy-conversion efficiency $\eta = 0.1$ (see Yu & Tremaine 2002), and derive luminosities in the various bands adopting standard spectral energy distributions following Marconi et al. (2004) in the X-ray and UV bands. The supermassive BH mass $m_{BH}$ grows mainly through accretion episodes as described above, besides coalescence with other BHs during galaxy merging. As an initial condition, we assume small seed BHs of mass $10^2 \, M_\odot$ (Madau & Rees 2001) to be initially present in all galaxy progenitors; our results are insensitive to the specific value as long as it is smaller than some $10^5 \, M_\odot$.

The radiation energy released by AGNs into the interstellar medium heat and expel part of the galactic gas (Cavaliere et al. 2002), as indicated, e.g., by the fast winds with velocities up to $10^{-1}c$ observed in the central regions of AGNs, likely originating from the acceleration of disk outflows by the AGN radiation field (see Begelman 2003 for a review). A detailed model for the transport of energy from the inner, outflow region to the larger scales has been developed by Lapi et al. (2005), and implemented into the R-SAM by Menci et al. (2008). Central, highly supersonic outflows compress the gas into a blast wave terminated by a leading shock front, which moves outward with a lower but still supersonic speed and sweeps out the surrounding medium. The key quantity determining all shock properties

is the total energy injected by AGNs into the surrounding gas $\Delta E = \epsilon_{AGN} \eta c^2 \Delta m_{acc} = \epsilon_{AGN} L \tau$. This is computed for each BH accretion episode in our Monte Carlo simulation; the value of the energy feedback efficiency for coupling with the surrounding gas is taken as $\epsilon_{AGN} = 5 \times 10^{-2}$, which is consistent with the values required to match the X-ray properties of the intracluster medium in clusters of galaxies (see Cavaliere et al. 2002). This is also consistent with the observations of wind speeds up to $v_w \sim 0.1c$ in the central regions, which yield $\epsilon_{AGN} \sim v_w/2c \sim 0.05$ by momentum conservation between photons and particles (see Chartas et al. 2002; Pounds et al. 2003); this value has also been adopted in a number of simulations (e.g., Di Matteo et al. 2005; Sijacki et al. 2007) and semi-analytic models of galaxy formation (e.g., Menci et al. 2006; see Hopkins et al. 2005b). The injection of energy $\Delta E$ (relative to the initial thermal energy content $E \propto m_c$ of the galactic gas) determines the Mach number $\mathcal{M} \approx (1 + \Delta E/E)^{1/2}$ (Lapi et al. 2005) of the expanding shock sweeping out the galactic gas surrounding the AGN. Thus, the expansion velocity of the blast wave, and hence the properties of the surrounding galactic gas, are directly related to the AGN luminosity. Note that in principle the same AGN feedback affects not only the galactic gas but also the halo hot gas. However, the key quantity in our treatment of the AGN feedback is the ratio $\Delta E/E$; since the thermal energy content of the hot halo gas is much larger than that of a single galaxy, the effect on the hot gas is smaller than that on the galaxies and does not affect our main results below.

The above modeling of AGN evolution in the framework of hierarchically evolving DM halos has been worked out in our previous papers to compare with a wide set of observations. The predicted local $M_{BH}$–$m_*$ relation has been successfully tested against observations in Lamastra et al. (2010); the description of AGN feedback yields an inverse luminosity dependence of the fraction of obscured AGNs (with column densities $N_H \geqslant 10^{22}$ cm$^{-2}$) which correctly reproduces the observed behavior (Menci et al. 2008); finally, the predicted abundance of high-luminosity AGNs agrees with the observed luminosity functions up to the highest redshifts ($z \approx 6$; see Menci et al. 2004, 2008). However, as discussed in the Introduction, the abundance of low-luminosity AGNs with X-ray luminosity $L_X \leqslant 10^{43}$ erg s$^{-1}$ at high redshifts ($z \geqslant 2$) is largely overpredicted by the model, independently of the tuning of free parameters (e.g., the feedback efficiency $\epsilon_{AGN}$), at least within the ranges allowed by consistency of the AGN and host galaxy properties with independent observables. In the following, we shall investigate the impact of a WDM spectrum on such a population of low-luminosity AGNs.

## 3. THE EVOLUTION OF THE AGN LUMINOSITY FUNCTIONS IN A WDM COSMOLOGY

To compute the evolution of the AGN luminosity function in the CDM and WDM, we first run Monte Carlo realizations of merging trees in both cosmologies as discussed in Section 2.1. Then we run the full SAM to model the baryonic physics in the generated DM halos, as described in Section 2.2; the model free parameters are the same as in our previous papers (Menci et al. 2005, 2006, 2008, 2012) in order to single out the effects of changing the DM spectrum with the same baryon physics.

We show the resulting evolution of the AGN luminosity function in Figure 1. Since we aim at investigating the effects of suppressing the power spectrum at small masses (hence at low AGN luminosities), we chose to show the distribution

of X-ray luminosities in the 2–10 keV band; this allows us to directly compare with X-ray observations, which are best suited to sample the population of low-luminosity AGNs. The predictions for the WDM case are represented by shaded areas, with the upper envelope corresponding to merger trees derived by directly extending the standard EPS theory to the WDM case, while the lower envelope of the area corresponds to assuming a sharp cutoff for the progenitor distributions (and halo mass functions) for $M \leqslant M_{fs}$ (see Sections 2.1 and 4 in Paper I).

While at low redshifts ($z \lesssim 1.5$) both the CDM and the WDM models provide acceptable fits to the observations (with WDM slightly underestimating the abundance of low-luminosity AGNs), at higher redshifts large differences arise at luminosities $L_{2-10\,keV} \lesssim 10^{44}$ erg s$^{-1}$. At such redshifts and luminosities, the CDM model yields luminosity functions appreciably steeper than observed; this behavior of CDM predictions is also shared by other recent semi-analytic models for the evolution of AGNs (Hirschmann et al. 2012; see also Shankar et al. 2010), so that it seems to constitute a common feature of most fiducial CDM models, although radically different assumptions like heavy initial BH seeds (Begelman et al. 2006; see also Khlopov et al. 2004) could still resolve the mismatch (see the Conclusions, Section 5). A better agreement is obtained in the WDM case, due to the suppression of the power spectrum at small scales (Equation (2)). This reduces the predicted density of low-luminosity AGNs since—in an interaction-driven model—low-luminosity AGNs are related either to low-mass galaxies accreting clumps of comparable mass (low values of the cold gas mass $m_c$; see the text between Equations (4)–(5)), or to larger galaxies interacting with clumps of much smaller mass (the $m'/m$ ratio in $f_{acc}$ in Equation (4)). In both cases, reducing the abundance of low-mass condensations through the adoption of a WDM model results in a flatter AGN luminosity function at the low-mass end. The effect is stronger at higher redshifts since CDM models predict low-mass galaxies to form mainly at early cosmic times, so that at $z \lesssim 2$ a substantial fraction of them has been included in larger galaxies; on the other hand, the (minor) fraction of low-mass galaxies that collapsed at $z \lesssim 2$ is characterized by lower gas densities (corresponding to lower escape velocities) and hence by a larger gas depletion due to supernovae feedback, which contributes to flatten the AGN luminosity function even in the CDM case. We expect the above effects to be quite general in interaction-driven scenarios for AGN fueling, since the $m'/m$ scaling of the destabilized gas (and of the related BH accretion; see, e.g., Hopkins & Quataert 2010) results not only from our model (see Equation (3)), but also from aimed hydrodynamical $N$-body simulations of galaxy merging (see Cox et al. 2008), while the direct scaling of $m_c$ with the galaxy mass is shared by all cosmological models of galaxy formation, as well as the feedback dependence on the escape velocity of galaxies. Note also that—at any redshift—for the luminous QSO population the effect of assuming a WDM spectrum is minimal. In fact, the large accretion rates characterizing such objects require the interactions of massive galaxies with clumps of comparable sizes, whose abundance is not sensibly affected by the small-scale cutoff in the DM power spectrum.

Thus, high-redshift ($z \geqslant 2$) measurements of the abundance of low-luminosity ($L_{2-10} \leqslant 10^{44}$) erg s$^{-1}$ AGNs are best suited to discriminate between the CDM and the WDM predictions. Such observations are now within reach of the recent deep searches. In particular, Fiore et al. (2012) exploited the combination of the multicolor catalogues MUSIC and ERS of the GOODS south field (Grazian et al. 2006, 2011) with 4 Ms
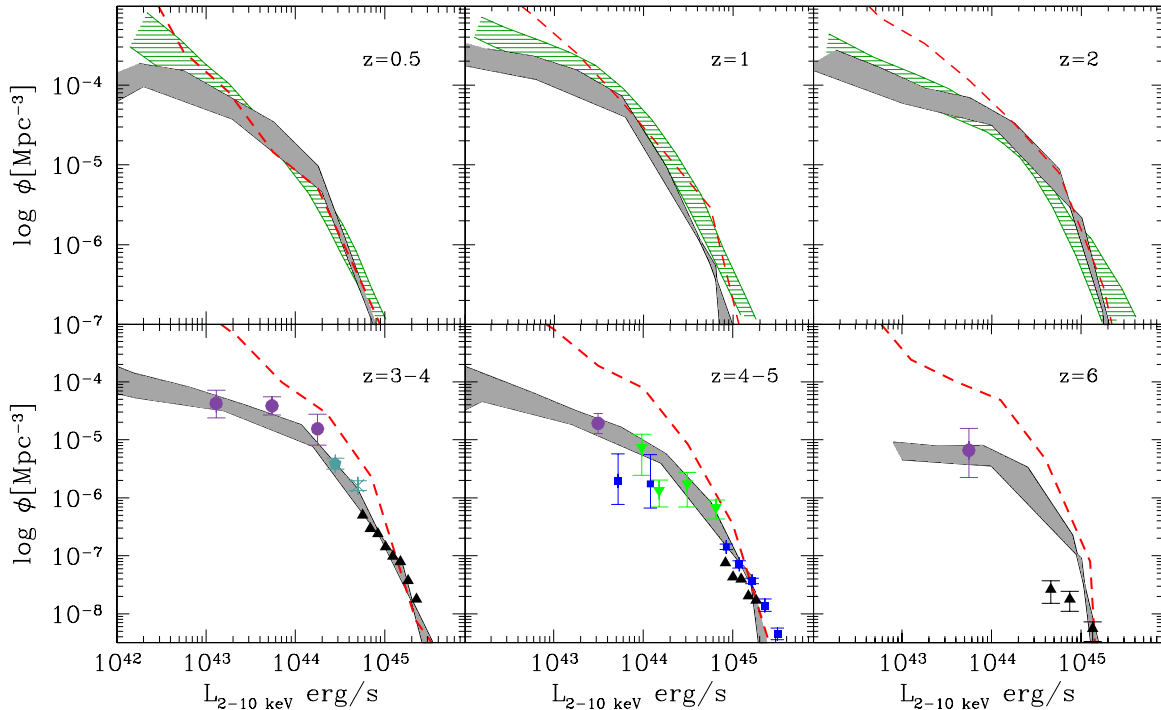
**Figure 1.** Evolution of the AGN luminosity function $\phi = dn/\log L$ (in the X-ray band 2–10 keV) predicted in WDM cosmology (the gray region) is compared with that corresponding to a CDM cosmology (dashed red line) and with the results of different observations; the upper envelope of the gray region correspond to WDM merging trees computed through direct application of the EPS theory with a WDM spectrum given in Equation (2), while the lower envelope corresponds to trees where the inclusion of halos with mass $M \leqslant M_{fs}$ is suppressed (see Section 2.1). The redshifts corresponding to the different panels are given in the labels. As for the observational data (all accounting for obscured objects), the hatched regions in the low-redshift bins ($z \leqslant 2$) bracket the observational estimates by La Franca et al. (2005), Ebrero et al. (2009), and Aird et al. (2010) and thus take into account systematic uncertainties of the different determinations. At higher redshifts we compare with X-ray observations of AGNs from *XMM*-COSMOS (Brusa et al. 2010; asterisk), *Chandra*-COSMOS (Civano et al. 2011; diamond), and *Chandra*-GOODS-MUSIC/ERS (Fiore et al. 2012; solid circles). These have been complemented with measurements derived from UV selected samples from the GOODS (Fontanot et al. 2007; solid squares), the Sloan survey (Richards et al. 2006 and Jiang et al. 2009; filled triangles), and the deep surveys analyzed by Glikman et al. (2011; inverted triangles), where the rest-frame 1450 Å luminosities have been converted to the 2–10 keV band using the bolometric corrections in Marconi et al. (2004).

(A color version of this figure is available in the online journal.)

*Chandra* images in the 2–10 KeV X-ray band to obtain the deepest measurements of low-luminosity AGNs. They selected faint AGN activity among the numerous Lyman-break galaxies in a wide redshift interval $3 < z < 7$, putting interesting constraints on the faint end of the luminosity function at $z = 3$–4, 4–5, and $z > 5.8$, which we show in the bottom panels of Figure 1. Note that such points account for obscured objects, including the Compton-thick fraction observed in the sample ($\sim 20\%$ for $z \gtrsim 3$); Fiore et al. (2012) estimated the uncertainty on the observed luminosity functions due to possibly undetected (or unaccounted-for) Compton-thick sources being small ($\lesssim 15\%$). Thus, the X-ray detections make the sample more complete with respect to the optical surveys and this is reflected in the higher densities attained by the Fiore et al. (2012) luminosity functions compared to extrapolations of their optical counterparts to low luminosities; nevertheless, for $L_{2-10} \leqslant 10^{44}$ erg s$^{-1}$, such number densities are overestimated by our fiducial CDM model by factors up to ten (in the lowest luminosity bins), while they are well matched by the WDM models. Thus, the indications from such deep, high-redshift observations is that the WDM scenario that provides a viable solution to the CDM overprediction of faint galaxies (see Paper I) could also provide an interesting framework for the evolution of the AGN population, at least in interaction-driven scenarios for the AGN triggering. As we shall show in Section 4, such a conclusion is quite robust with respect to the choice of the supernovae feedback parame-

ters, the main source of uncertainty at the faint end of the AGN luminosity function in semi-analytic models.

Finally, we note that the correlation between the galactic and the AGN properties is not strongly affected by the shape of the DM power spectrum on small scales. This is shown in Figure 2, where we compare the local BH–stellar mass relations predicted in the CDM and WDM scenarios with available data (details on the comparison are given in Lamastra et al. 2010, where we presented the CDM predictions). The only appreciable difference is the smaller scatter (for small values of $M_{BH}$) in the WDM case, due to the smaller number of interactions with low-mass galaxies, largely affecting the accretion history of low-mass BHs. The predicted evolution of the BH–stellar mass relation is also weakly dependent on the adopted power spectrum: this is illustrated by the paths showing the growth of BH mass relative to the stellar mass for largest BHs in our Monte Carlo simulation. As predicted for CDM in our previous work (see Lamastra et al. 2010), the local relation is reached—for massive objects—through paths passing *above* the local relation, indicating a faster growth of BH masses compared to stellar masses in the earliest phase of galaxy evolution, in both the CDM and the WDM case.

## 4. DISCUSSION: THE ROLE OF GALAXY FEEDBACK

In the previous section we have shown that the recent observational estimates of the high-redshift AGN luminosity
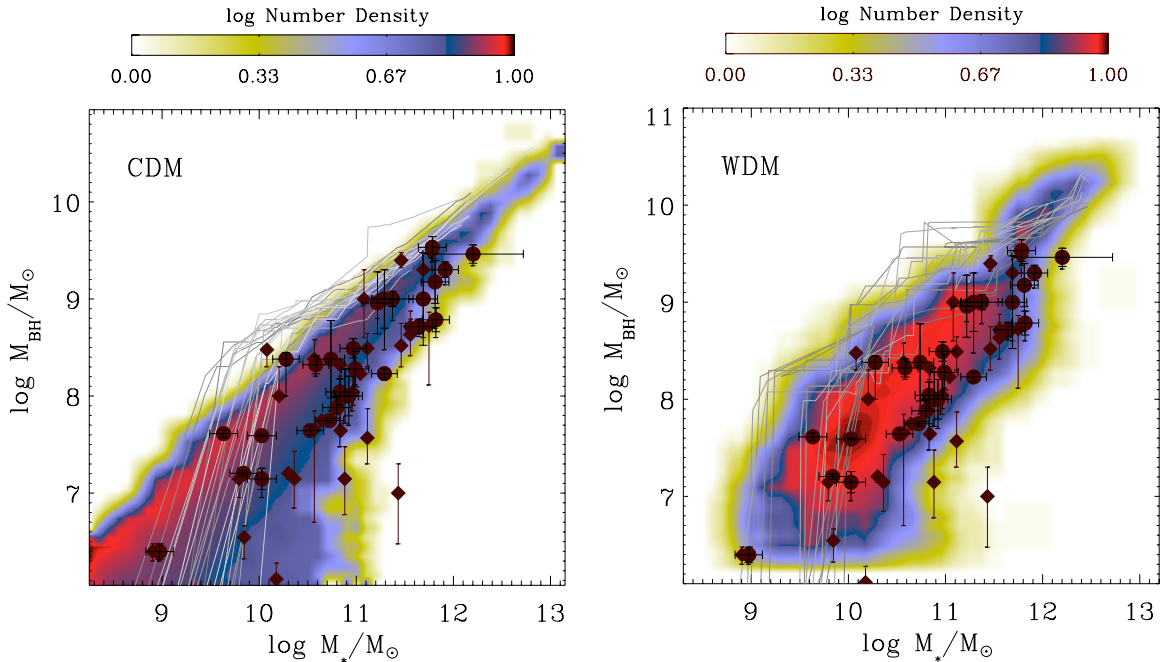
**Figure 2.** Local predicted $M_{BH}-M_*$ relation for the CDM (left panel) and the WDM (right panel) cosmology is compared with data by Häring & Rix (2004; diamonds), and Marconi & Hunt (2003; squares); the color code represents the logarithm of the space density of BHs in a given $M_{BH}-M_*$, normalized to the maximum value, as indicated by the upper color bar. We also show some of the paths in the $M_{BH}(t)-M_*(t)$ plane followed, during their evolution, by BHs (and by their host galaxies), reaching a final mass of $M_{BH}(z=0) \geqslant 10^{10} M_\odot$.

(A color version of this figure is available in the online journal.)

functions are matched by the model predictions in WDM cosmology, due to the suppression of the *number density* of low-mass galaxies at high redshifts. It is interesting to investigate whether a similar agreement can be achieved through a proper *luminosity evolution* within the standard CDM scenario. This would require a suppression of the AGN luminosities for $L_X \lesssim 10^{44}$ erg s$^{-1}$ at redshift $z \gtrsim 3$. Here we investigate whether increasing the efficiency and the mass dependence of the stellar feedback can help in bringing the CDM predictions in closer agreement with present data on the AGN abundance at high redshifts.

To this aim, we modified our fiducial CDM model by maximizing the feedback efficiency at small galaxy masses. Our *maximal feedback* model differs from our fiducial case in three respects: (1) the (inverse) scaling of the galaxy feedback on the circular velocity is increased from $\dot{m}_{hot} \propto v_c^{-2}$ (see Section 2.2) to $\dot{m}_{hot} \propto v_c^{-4}$; (2) the supernovae efficiency is increased to $\epsilon = 0.03$; (3) an artificial cutoff for gas cooling is assumed for galaxy halos with circular velocity larger than 250 km s$^{-1}$; this mimics the effect of the AGN radio mode implemented in several SAMs to fit the bright end of the local luminosity functions (the chosen value for the cutoff circular velocity corresponds to that resulting from the analysis of Fontanot et al. 2011). Although such a point constitutes a critical issue in galaxy formation models, it has a minor influence on the evolution of the low-mass end of the galaxy and AGN luminosity functions

Such a *high-feedback* model is similar to other semi-analytic models, like that by Guo et al. (2011), who adopt a similar scaling for the SN feedback. In fact, it provides an excellent fit to the low-redshift stellar mass distribution and luminosity function (see Figures 3(a) and (b)), similar to that provided by our WDM model; even though it is well known that such high-feedback models in CDM cosmology yield an exceeding

fraction of faint red galaxies at low redshift (see also Guo et al. 2011; Lo Faro et al. 2009), we shall investigate such a case to probe the effects of changing the galaxy feedback on the AGN evolution, and to bracket the range of CDM predictions corresponding to different SAMs in the literature (within the assumption of interaction-triggered AGN fueling).

The evolution of the AGN luminosity functions in the above "maximal-feedback" model is shown in the bottom panels of Figure 3, where we also show for comparison the results for the WDM (solid line) and the fiducial CDM model (dotted). Note that, while at low redshifts the CDM maximal feedback model provides an excellent match to the data, at redshifts $z \gtrsim 3.5$ the implementation of a maximal feedback does not seem able to properly match the observed abundance of low-luminosity AGNs (those in the faintest bin $L_{2-10} \leqslant 5\,10^{43}$ erg s$^{-1}$). This is due to a twofold reason: (1) the inner density of DM halos rapidly grows with redshifts, so that for $z \gtrsim 2$ the escape velocity of DM halos $\propto \rho^{1/3}$ remains large even for low-mass galaxies, and this, in turn, suppresses the feedback efficiency in removing gas from the cold phase. This effect has already been found and discussed by, e.g., Lo Faro et al. (2009), who found that SAMs in CDM cosmology overpredict the slope of the low-mass end of the stellar mass distribution at high redshifts ($z \gtrsim 2$) even in the presence of a large feedback efficiency; this effect is also responsible for the overprediction of low-mass galaxies at $z \gtrsim 1$ in the SAM by Guo et al. (2011) based on the Millennium simulation. (2) In interaction-driven models for the AGN feeding, faint AGNs at high redshifts are associated with minor mergers, rather than being produced by gas-poor galaxies; to reduce the abundance of faint AGNs with respect to the fiducial CDM case, the suppression of the number density of low-mass galaxies (and hence of minor mergers) resulting in WDM cosmology is more efficient than reducing the cold gas fractions by increasing the stellar feedback.
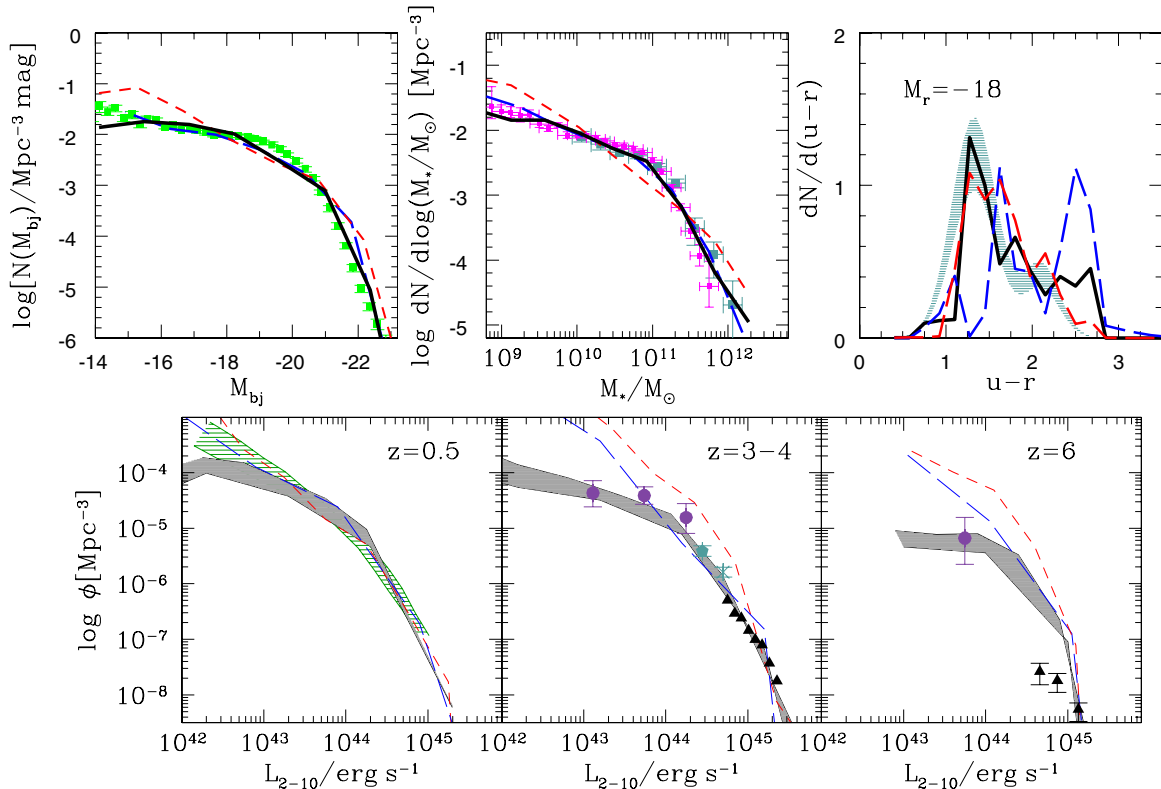
**Figure 3.** Top left: the local galaxy luminosity function ($b_j$-band) in the WDM model (solid line) compared to our maximal feedback CDM model (see the text; long-dashed blue line); we also show the corresponding prediction for our fiducial CDM model (short-dashed red line): the data points are from the 6dF Galaxy Survey (Jones et al. 2006); for the sake of readability, only the WDM model derived from direct extension of EPS (see Section 2.1) is shown. Top middle: the local stellar mass distribution: the different models correspond to line types as in the previous panel. Data points are from Drory et al. (2004; squares) and Fontana et al. (2006; circles). Top right: the $u - r$ color distribution of faint ($M_r = -18$) galaxies in the different models (line types as in previous panels) is compared with the Sloan data (from Baldry et al. 2004; hatched area). Bottom panels: the evolution of the AGN luminosity function (in the X-ray band 2–10 keV) predicted in WDM models (gray region, as in Figure 1) is compared with that corresponding to our *maximal feedback* CDM model (long-dashed blue line) to our fiducial CDM model (short-dashed red line) and to the results of different observations. The redshifts corresponding to the different panels are given in the labels. Data hatched region and data points as in Figure 1.

(A color version of this figure is available in the online journal.)

Thus, at high redshifts ($z \gtrsim 2$) the CDM overprediction of low-mass galaxies yielded by CDM models (see Lo Faro et al. 2009; Guo et al. 2011; Somerville et al. 2008) seems to have a counterpart in the excess of the number of predicted faint AGNs even assuming a maximal feedback efficiency; this makes the number density effects of the WDM scenario an attractive alternative for all models aiming at providing a unified solution to the different aspects of the CDM overabundance problem.

## 5. CONCLUSIONS

We have shown that the recent measurements of the abundance of low-luminosity ($L_X \leqslant 10^{44}$ erg s$^{-1}$) AGNs at high redshifts ($z \geqslant 4$) can provide severe constraints to models connecting the AGN evolution to galaxy formation through the effects of galaxy interactions. In particular, the long-standing problem of CDM overprediction of low-mass galaxies at such high redshifts reflects a similar excess of low-luminosity AGNs. We have shown that the suppression of the number of low-mass galaxies obtained in a WDM model (with WDM particles of mass $m_X \approx 1$ keV) provides a viable solution to both the galactic (Menci et al. 2012) and the AGN (this paper) excess. We have also shown that solutions to such excess based on increased supernovae feedback are less efficient than the WDM suppression of low-mass galaxies, at least in interaction-driven models for the triggering of AGNs; in fact, in such models, faint AGNs at

high redshifts are associated with minor mergers, rather than being produced by gas-poor galaxies; to reduce the abundance of faint AGNs with respect to the fiducial CDM case, the suppression of the number density of low-mass galaxies (and hence of minor mergers) resulting in WDM cosmology is more efficient than reducing the cold gas fractions by increasing the stellar feedback. Note however that, when the WDM merging trees are computed with progenitor distributions and halo mass functions strongly suppressed below the free-streaming scale (as suggested by Benson et al. 2013), the low-redshift AGN luminosity function underpredicts the observations at low luminosities ($L_{2-10} \leqslant 10^{43}$ erg s$^{-1}$; see Figure 1).

While the strongest constraints to distinguish between WDM and CDM models are naturally given by the faint ($L_X \leqslant 10^{44}$ erg s$^{-1}$) end of the AGN luminosity function at $z \geqslant 4$, faint AGNs at high-$z$ is of course the region of the AGN parameter space most difficult to probe. The measurements of the faint end of the AGN luminosity function in Figures 1 and 3 are reasonably good at $z = 3$–4, but they are rather loose at $z > 4$. In particular, as noted by Fiore et al. (2012) the point at $z = 6$ should be regarded as an upper limit to the AGN density rather than a determination, being based on just two galaxies, detected in the small ERS area within the CDFS region, with rather loosely constrained photometric redshift. As of today we do not have a single AGN at $z > 6$ with a robust spectroscopic redshift.

This poor situation may improve in the next few years. At the flux limits reached by the deepest *Chandra* exposure (4 Ms), there are several hundreds of AGNs/deg$^2$ for $z > 4$, $\sim$100 AGNs/deg$^2$ for $z > 5$, and <100 AGNs/deg$^2$ for $z > 5.8$. It is clear that to obtain a more robust demography of the $z > 6$ AGNs, a search in a much wider area, such as the CANDELS area (Grogin et al. 2011; Koekemoer et al. 2011), is mandatory, and requires spectroscopic confirmation of the X-ray emitting, candidate $z > 6$ galaxies. The CANDELS deep and wide surveys cover a total of 130 arcmin$^2$ and 670 arcmin$^2$ to a depth of $H = 27.8$ and $H \sim 26.5$, respectively, about 3 times and 12 times the ERS area. The two candidate $z > 6$ ERS galaxies detected by *Chandra* in the ERS field are faint $H = 26.6$ and $H = 27$ sources. The GOODS source with $z > 7$ in the Luo et al. (2010) catalog has $H = 27.6$. In summary, we expect <5 AGNs in the CANDELS deep survey for $z > 6$ and less than 20 AGNs for $z > 6$ in the CANDELS wide survey. We note that a fraction of these sources will be at the limit of, or below, the $H$ band sensitivity threshold of the wide survey. As of today, *Chandra* has spent of the order of 8 Ms on the CANDELS fields, most of them on the CANDELS deep fields. To reach the sensitivity to detect the faint $z > 6$ AGN in the wide area, and additional 5–6 Ms are needed. This is within reach of the *Chandra* observatory in the next few years.

Note that our results do not exclude that the CDM predictions for the number low-luminosity AGN at high redshifts can be reconciled with observations provided: (1) less luminous AGNs are driven by secular processes rather than by galaxy interactions; (2) additional baryonic physics is involved in the BH accretion at high redshifts (especially for low-luminosity AGNs); (3) heavy initial BH seeds are assumed. Such processes could provide the negative AGN luminosity evolution needed to balance the AGN excess of standard CDM models. Indeed, some of the above conditions have been explored in recent semi-analytic models. As for the first possibility (point (1)) above), both Fanidakis et al. (2012) and Hirschmann et al. (2012) also include disk instabilities as an additional trigger for BH accretion, with the former paper also including accretion at low rates from hot halos. While such models provide excellent fits to the AGN luminosity functions at $z \leqslant 4$, at higher redshifts ($z \gtrsim 4$) they predict different abundances for low-luminosity AGNs; while the predictions shown in Fanidakis et al. (2012) are consistent with observations, the Hirschmann et al. (2012) model overestimates the abundance of faint AGNs. Here the critical issue is the luminosity range where the different accretion modes take over; in this respect, important hints to improve modeling will be provided by observations relating the AGN luminosity with galaxy mergers (see Treister et al. 2012) and with giant clumps associated to disk instabilities (see Bournaud et al. 2012) as well as by aimed *N*-body simulations (see, e.g., Bournaud et al. 2011).

As for the second and third possibilities (points (2)) and (3)) above), they are still open; indeed, Hirschmann et al. (2012) have shown that assuming a varying sub-Eddington limit (that depends on the cold gas fraction) and heavy BH seeds with a tuned cutoff for the host halo mass can resolve the mismatch. However, while varying sub-Eddington limit onto low-mass BHs at high redshifts and heavy BH seeds could solve the CDM excess of predicted low-luminosity AGNs, they would leave unchanged its overprediction of low-mass/faint galaxies at high redshifts ($z \gtrsim 3$), which should find a different solution. Indeed, our results strongly indicate that, when seeking a unified a solution to the CDM overprediction of low-luminosity AGNs

and of low-mass galaxies at $z \geqslant 3$, the WDM cosmology represents an appealing solution.

## REFERENCES

Abadi, M. G., Navarro, J. F., Steinmetz, M., & Eke, V. R. 2003, ApJ, 591, 499
Aird, J., Nandra, K., Laird, E. S., et al. 2010, MNRAS, 401, 2531
Bahcall, J. N., Kirhakos, S., Saxe, D. H., & Schneider, D. P. 1997, ApJ, 479, 642
Baldry, I. K., Glazebrook, K., Brinkmann, J., et al. 2004, ApJ, 600, 681
Bardeen, J. M., Bond, J. R., Kaiser, N., & Szalay, A. S. 1986, ApJ, 304, 15
Barkana, R., Haiman, Z., & Ostriker, J. P. 2001, ApJ, 558, 482
Baugh, C. M. 2006, RPPh, 69, 3101
Begelman, M. C. 2003, in Coevolution of Black Holes and Galaxies, Carnegie Observatories Astrophysics Series, Vol. 1, ed. L. C. Ho (Cambridge: Cambridge Univ. Press)
Begelman, M., Volonteri, M., & Rees, M. J. 2006, MNRAS, 370, 289
Bennert, N., Canalizo, G., Jungwiert, B., et al. 2008, ApJ, 677, 846
Benson, A. J., de Haan, I., Dudley, J. P., et al. 2013, ApJ, 763, 147
Benson, A. J., Frenk, C. S., Lacey, C. G., Baugh, C. M., & Cole, S. 2002, MNRAS, 333, 177
Bode, P., Ostriker, J. P., & Turok, N. 2001, ApJ, 556, 93
Bond, J. R., Cole, S., Efstathiou, G., & Kaiser, N. 1991, ApJ, 379, 440
Bond, J. R., Szalay, A. S., & Turner, M. S. 1982, PhRvL, 48, 1636
Bower, R. G., Benson, A. J., Malbon, R., et al. 2006, MNRAS, 370, 645
Boyle, B. J., Shanks, T., Croom, S. M., et al. 2000, MNRAS, 317, 1014
Bournaud, F., Dekel, A., Teyssier, R., et al. 2011, ApJL, 741, L33
Bournaud, F., Juneau, S., Le Floc'h, E., et al. 2012, ApJ, 757, 81
Brusa, M., Civano, F., Comastri, A., et al. 2010, ApJ, 716, 348
Canalizo, G., & Stockton, A. 2001, ApJ, 555, 719
Cattaneo, A., Dekel, A., Devriendt, J., Guiderdoni, B., & Blaizot, J. 2006, MNRAS, 370, 1651
Cavaliere, A., Lapi, A., & Menci, N. 2002, ApJL, 581, L1
Cavaliere, A., & Vittorini, V. 2000, ApJ, 543, 599
Chartas, G., Brandt, W. N., Gallagher, S. C., & Garmire, G. P. 2002, ApJ, 579, 169
Ciotti, L. 2009, Natur, 460, 333
Cirasuolo, M., McLure, R. J., Dunlop, J. S., et al. 2010, MNRAS, 401, 1166
Civano, F., Brusa, M., Comastri, A., et al. 2011, ApJ, 741, 91
Cole, S. 2005, MNRAS, 362, 505
Cole, S., Aragon-Salamanca, A., Frenk, C. S., Navarro, J. F., & Zepf, S. E. 1994, MNRAS, 271, 781
Cole, S., Lacey, C. G., Baugh, C. M., & Frenk, C. S. 2000, MNRAS, 319, 168
Colombi, S., Dodelson, S., & Widrow, L. M. 1996, ApJ, 458, 1
Cox, T. J., Jonsson, P., Somerville, R. S., Primack, J. R., & Dekel, A. 2008, MNRAS, 384, 386
Croom, S. M., Richards, G. T., Shanks, T., et al. 2009, MNRAS, 399, 1755
Croton, D. J., Springel, V., White, S. D. M., et al. 2006, MNRAS, 365, 11
de Vega, H. J., & Sanchez, N. G. 2012, PhRevD, 85, 3518
De Lucia, G., & Blaizot, J. 2007, MNRAS, 375, 2
De Lucia, G., Boylan-Kolchin, M., Benson, A. J., Fontanot, F., & Monaco, P. 2010, MNRAS, 406, 1533
Dekel, A., & Silk, J. 1986, ApJ, 303, 39
Di Matteo, T., Springel, V., & Hernquist, L. 2005, Natur, 433, 604
Drory, N., Bender, R., Feulner, G., et al. 2004, ApJ, 608, 742
Ebrero, J., Carrera, F. J., Page, M. J., et al. 2009, A&A, 493, 55
Fan, X., Hennawi, J. F., Richards, G. T., et al. 2004, AJ, 128, 515
Fan, X., Narayanan, V. K., Lupton, R. H., et al. 2001, AJ, 122, 2833
Fanidakis, N., Baugh, C. M., Benson, A. J., et al. 2012, MNRAS, 419, 2797
Ferrarese, L., & Merritt, D. 2000, ApJL, 539, L9
Fiore, F., Puccetti, S., Grazian, A., et al. 2012, A&A, 537, 22
Fisher, K. B., Bahcall, J. N., Kirhakos, S., & Schneider, D. P. 1996, ApJ, 468, 496
Fontana, A., Salimbeni, S., Grazian, A., et al. 2006, A&A, 459, 745
Fontanot, F., Cristiani, S., Monaco, P., et al. 2007, A&A, 461, 39
Fontanot, F., De Lucia, G., Monaco, P., Somerville, R. S., & Santini, P. 2009, MNRAS, 397, 1776
Fontanot, F., Pasquali, A., De Lucia, G., et al. 2011, MNRAS, 413, 957
Gebhardt, K., Bender, R., Bower, G., et al. 2000, ApJL, 539, L13
Gentile, G., Tonini, C., & Salucci, P. 2007, A&A, 467, 925
Glikman, E., Djorgovski, S. G., Stern, D., et al. 2011, ApJL, 728, L26
Grazian, A., Castellano, M., Koekemoer, A. M., et al. 2011, A&A, 532, 33

Grazian, A., Fontana, A., de Santis, C., et al. 2006, A&A, 449, 951
Grogin, N. A., Kocevski, D. D., Faber, S. M., et al. 2011, ApJS, 197, 35
Guo, Q., White, S., Boylan-Kolchin, M., et al. 2011, MNRAS, 413, 101
Häring, N., & Rix, H.-W. 2004, ApJL, 604, L89
Hartwick, F. D. A., & Shade, D. 1990, ARA&A, 28, 437
Hasinger, G., Miyaji, T., & Schmidt, M. 2005, A&A, 441, 417
Hennawi, J. F., Strauss, M. A., Oguri, M., et al. 2006, AJ, 131, 1
Henriques, B., Maraston, C., Monaco, P., et al. 2011, MNRAS, 415, 3571
Hirschmann, M., Somerville, R. S., Naab, T., & Burkert, A. 2012, MNRAS, 426, 237
Ho, L. C. 1999, in Observational Evidence for Black Holes in the Universe, ed. S. K. Chakrabarti (Dordrecht: Kluwer), 157
Hopkins, P. F., Cox, T. J., Kere, D., & Hernquist, L. 2008, ApJS, 175, 390
Hopkins, P. F., Hernquist, L., Cox, T. J., et al. 2005a, ApJ, 630, 705
Hopkins, P. F., Hernquist, L., Cox, T. J., et al. 2005b, ApJ, 632, 81
Hopkins, P. F., Hernquist, L., Cox, T. J., et al. 2006, ApJS, 163, 1
Hopkins, P. F., & Quataert, E. 2010, MNRAS, 407, 1529
Jiang, L., Fan, X., Bian, F., et al. 2009, AJ, 138, 305
Jones, D. H., Peterson, B. A., Colless, M., & Saunders, W. 2006, MNRAS, 396, 535
Kauffmann, G., & Haehnelt, M. 2000, MNRAS, 311, 576
Kauffmann, G., White, S. D. M., & Guiderdoni, B. 1993, MNRAS, 264, 201
Khlopov, M. Y., Rubin, S. G., & Sakharov, A. S. 2004, APh, 23, 265
Klypin, A., Kravtsov, A. V., Valenzuela, O., & Prada, F. 1999, ApJ, 522, 82
Koekemoer, A. M., Faber, S. M., Ferguson, H. C., et al. 2011, ApJS, 197, 36
Kormendy, J., & Bender, R. 2009, ApJL, 691, L142
Kormendy, J., & Richstone, D. 1995, ARA&A, 33, 581
Kusenko, A. 2009, PhR, 481, 1
Lacey, C., & Cole, S. 1993, MNRAS, 262, 627
La Franca, F., Fiore, F., Comastri, A., et al. 2005, ApJ, 635, 864
Lamastra, A., Menci, N., Maiolino, R., Fiore, F., & Merloni, A. 2010, MNRAS, 405, 29
Lapi, A., Cavaliere, A., & Menci, N. 2005, ApJ, 619, 60
Lapi, A., Shankar, F., Mao, J., et al. 2006, ApJ, 650, 42
Lo Faro, B., Monaco, P., Vanzella, E., et al. 2009, MNRAS, 399, 827
Lovell, M. R., Eke, V., Frenk, C. S., et al. 2012, MNRAS, 420, 2318
Luo, B., Brandt, W. N., Xue, Y. Q., et al. 2010, ApJS, 187, 560
Madau, P., Diemand, J., & Kuhlen, M. 2008, ApJ, 679, 1260
Madau, P., & Rees, M. J. 2001, ApJL, 551, L27
Magorrian, J., Tremaine, S., Richstone, D., et al. 1998, AJ, 115, 2285
Marchesini, D., van Dokkum, P. G., Förster Schreiber, N. M., et al. 2009, ApJ, 701, 1765
Marconi, A., & Hunt, L. K. 2003, ApJL, 589, L21
Marconi, A., Risaliti, G., Gilli, R., et al. 2004, MNRAS, 351, 169
Marulli, F., Bonoli, S., Branchini, E., Moscardini, L., & Springel, V. 2008, MNRAS, 385, 1846
Mateo, M. 1998, ARA&A, 36, 435
McGaugh, S. S., de Blok, W. J. G., Schombert, J. M., Kuzio de Naray, R., & Kin, J. H. 2007, ApJ, 659, 149
Menci, N., Cavaliere, A., Fontana, A., Giallongo, E., & Poli, F. 2002, ApJ, 578, 18
Menci, N., Cavaliere, A., Fontana, A., Giallongo, E., & Poli, F. 2004, ApJ, 604, 12
Menci, N., Cavaliere, A., Fontana, A., et al. 2003, ApJL, 587, L63
Menci, N., Fiore, F., & Lamastra, A. 2012, MNRAS, 421, 2384 (Paper I)
Menci, N., Fiore, F., Puccetti, S., & Cavaliere, A. 2008, ApJ, 686, 219
Menci, N., Fontana, A., Giallongo, E., Grazian, A., & Salimbeni, S. 2006, ApJ, 647, 753
Menci, N., Fontana, A., Giallongo, E., & Salimbeni, S. 2005, ApJ, 632, 49
Monaco, P., Fontanot, F., & Taffoni, G. 2007, MNRAS, 375, 1189
Moore, B., Quinn, T., Governato, F., Stadel, J., & Lake, G. 1999, MNRAS, 310, 1147
Myers, A. D., Richards, G. T., Brunner, R. J., et al. 2008, ApJ, 678, 635
Natarajan, P. 1999, ApJ, 512, 105
Peebles, P. J. E. 1982, ApJ, 258, 415
Peebles, P. J. E. 1993, Principles of Physical Cosmology (Princeton: Princeton Univ. Press)
Pounds, K., King, A. R., Page, K. L., & O'Brien, P. T. 2003, MNRAS, 346, 1025
Reed, D., Governato, F., Verde, L., et al. 2005, MNRAS, 357, 82
Richards, G. T., Strauss, M. A., Fan, X., et al. 2006, AJ, 131, 2766
Salimbeni, S., Giallongo, E., Menci, N., et al. 2008, A&A, 477, 763
Sanders, D. B., & Mirabel, I. F. 1996, ARA&A, 34, 749
Santini, P., Rosario, J. D., Shao, L., et al. 2012, A&A, 540, 109
Saslaw, W. C. 1985, Gravitational Physics of Stellar and Galactic Systems (Cambridge: Cambridge Univ. Press)
Serber, W., Bahcall, N., Ménard, B., & Richards, G. 2006, ApJ, 643, 68
Shankar, F., Bernardi, M., & Haiman, Z. 2009a, ApJ, 694, 867
Shankar, F., Crocce, M., Miralda-Escude, J., Fosalba, P., & Weinberg, D. H. 2010, ApJ, 718, 231
Shankar, F., & Mathur, S. 2007, ApJ, 660, 1051
Shankar, F., Weinberg, D. H., & Miralda-Escude, J. 2009b, ApJ, 690, 20
Shen, Y. 2009, ApJ, 704, 89
Sheth, R. K., Mo, H. J., & Tormen, G. 2001, MNRAS, 323, 1
Shin, M. S., Ostriker, J. P., & Ciotti, L. 2010, ApJ, 711, 268
Sijacki, D., Springel, V., Di Matteo, T., & Hernquist, L. 2007, MNRAS, 380, 877
Smith, R. E., & Markovic, K. 2011, PhRevD, 84, 3507
Somerville, R. 2002, ApJ, 572, 23
Somerville, R. S., Hopkins, P. F., Cox, T. J., Robertson, B. E., & Hernquist, L. 2008, MNRAS, 391, 481
Somerville, R. S., & Primack, J. R. 1999, MNRAS, 310, 1087
Spergel, D. N., Bean, R., Doré, O., et al. 2007, ApJS, 170, 377
Springel, V. 2005, Natur, 435, 629
Strand, N. E., Brunner, R. J., & Myers, A. D. 2008, ApJ, 688, 180
Treister, E., Schawinski, K., Urry, C. M., & Simmons, B. D. 2012, ApJL, 758, L39
Ueda, Y., Akiyama, M., Ohta, K., & Miyaji, T. 2003, ApJ, 598, 886
Viel, M., Becker, G. D., Bolton, J. S., et al. 2008, PhRvD, 100, 041304
Viel, M., Legourgues, J., Haenhelt, M. G., Matarrese, S., & Riotto, A. 2005, PhRvD, 71, 063534
Wyithe, J. S. B., & Loeb, A. 2003, ApJ, 586, 693
Yu, Q., & Tremaine, S. 2002, MNRAS, 335, 965